A Journal of the Gesellschaft Deutscher Chemiker

Angewandte International Edition

GDCh

Chemie

www.angewandte.org

Accepted Article

Title: Nanoscale Metal-organic Frameworks Mediate Photodynamic Therapy and Deliver CpG Oligodeoxynucleotides to Enhance Antigen Presentation and Cancer Immunotherapy

Authors: Kaiyuan Ni, Taokun Luo, Guangxu Lan, August Culbert, Yang Song, Tong Wu, Xiaoming Jiang, and Wenbin Lin

To be cited as: *Angew. Chem. Int. Ed.* 10.1002/anie.201911429
Angew. Chem. 10.1002/ange.201911429

Link to VoR: http://dx.doi.org/10.1002/anie.201911429
http://dx.doi.org/10.1002/ange.201911429

WILEY-VCH

10.1002/anie.201911429

WILEY-VCH

COMMUNICATION

Nanoscale Metal-organic Frameworks Mediate Photodynamic Therapy and Deliver CpG Oligodeoxynucleotides to Enhance Antigen Presentation and Cancer Immunotherapy

Kaiyuan Ni, Taokun Luo, Guangxu Lan, August Culbert, Yang Song, Tong Wu, Xiaomin Jiang, and Wenbin Lin*

Abstract: Checkpoint blockade immunotherapy (CBI) awakes host innate immune system and reactivates cytotoxic T cells to elicit durable response in some cancer patients. Herein we report the use of a cationic nanoscale metal-organic framework, W-TBP, to facilitate tumor antigen presentation by enabling immunogenic photodynamic therapy (PDT) and promoting the maturation of dendritic cells (DCs). Comprised of dinuclear W^{VI} secondary building units and photosensitizing 5,10,15,20-tetra(*p*-benzoato)porphyrin (TBP) ligands, cationic W-TBP mediates PDT to release tumor associated antigens and delivers immunostimulatory CpG oligodeoxynucleotides to DCs. The enhanced antigen presentation synergizes with CBI to expand and reinvigorate cytotoxic T cells, leading to superb anticancer efficacy and robust abscopal effects with >97% tumor regression in a bilateral breast cancer model.

Immunotherapy has emerged as a highly effective cancer treatment by harnessing the power of host immune system to recognize and eradicate tumors.[1] In particular, by targeting T lymphocyte regulatory pathways such as the PD-1/PD-L1 axis with neutralizing antibodies to reinvigorate cytotoxic T cells, checkpoint blockade immunotherapy (CBI) has enjoyed significant clinical success for several tumor types.[2] In addition to blocking immunosuppressive checkpoints, the generation of an effective anti-cancer immune response also depends on the release of tumor-associated antigens (TAAs) and their capture and presentation to T cells by antigen-presenting cells (APCs), particularly dendritic cells (DCs).[3] It is believed that the lack of TAAs in tumor microenvironments (TMEs) and ineffective antigen presentation by DCs contribute to CBI failure in the majority of cancer patients.[4]

One strategy to enhance antigen presentation is through the use of photodynamic therapy (PDT), in which a photosensitizer (PS) is administered to a patient followed by activation of the PS with light to generate highly cytotoxic $^1O_2$ to kill cancer cells.[5] PDT treatment is highly immunogenic and has the potential to recruit DCs to the TME by inducing calreticulin (CRT) exposure and releasing tumor cell debris, including TAAs.[6] Another strategy for promoting antigen presentation is through exposure of DCs to toll-like receptor (TLR) agonists, such as immunostimulatory CpG oligodeoxynucleotides for DC maturation via binding to TLR 9.[7] However, enzymatic degradation and inefficient cellular internalization of anionic CpG present major hurdles to the effective DC activation in vivo.[8] We surmise that a cationic nanoscale metal-organic framework (nMOF) can facilitate tumor antigen presentation by DCs via enabling immunogenic PDT and delivering anionic CpGs.

As a class of molecular nanomaterials, nMOFs are well suited for biomedical applications due to their crystallinity, tunability, and porosity.[9] For example, nMOFs have emerged as novel nanophotosensitizers for PDT with high PS loadings and facile ROS diffusion through their porous structures.[10] nMOFs have also provided effective vehicles for delivering small molecule drugs[11], proteins[12], and oligonucleotides[13]. Herein, we report the synthesis of a W-based nMOF, W-TBP, for efficient PDT and CpG delivery. In addition to mediating PDT to release TAAs, cationic W-TBP efficiently adsorbs anionic CpGs and facilitates their internalization by DCs to promote DC maturation. The enhanced antigen presentation synergizes with CBI to elicit strong antitumor immunity with >97% tumor regression in a bilateral breast cancer model (Scheme 1).

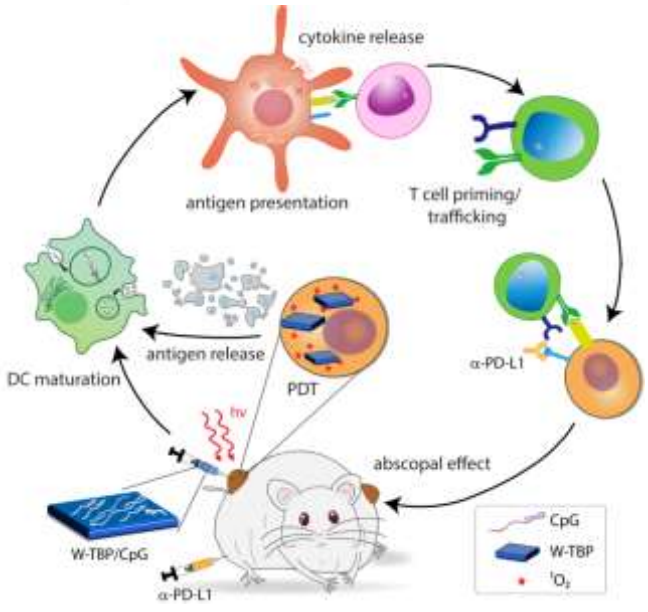

Scheme 1. W-TBP/CpG promoted antigen presentation via immunogenic PDT and CpG delivery synergizes with CBI to afford systemic antitumor immunity.

W-TBP and Bi-TBP nMOFs were synthesized through solvothermal reactions between 5,10,15,20-tetra(*p*-benzoato)-porphyrin (H_4TBP) and WCl_6 or $Bi(NO_3)_3{\cdot}5H_2O$ in N,N-dimethylformamide and acetic acid at 80 ºC. TEM imaging revealed similar rectangular nanoplate-like morphologies (Figure 1a&1b) with a width of ~100 nm and length of ~200 nm for both W-TBP (Figure 1c) and Bi-TBP (Figure 1d). High resolution TEM

K. Ni, T. Luo, G. Lan, A. Culbert, Y. Song, T. Wu, X. Jiang, Prof. W. Lin
Department of Chemistry, The University of Chicago
929 East 57th street, Chicago, Illinois 60637, United States
E-mail: wenbinlin@uchicago.edu
Prof. W. Lin
Department of Radiation and Cellular Oncology and The Ludwig Center for Metastasis Research, The University of Chicago
Chicago, Illinois 60637, United States

Supporting information for this article is given via a link at the end of the document.

10.1002/anie.201911429

WILEY-VCH

COMMUNICATION

(HRTEM) imaging and fast Fourier transform (FFT) patterns of both W-TBP and Bi-TBP revealed similar 4-fold symmetry (Figure 1e&1f), consistent with the projection of their structures along the (010) and (100) directions, respectively (Figure S1-2). The distance between adjacent lattice points in HRTEM measured ~1.6 nm, matching the distance between the centers of adjacent SBUs. Atomic force microscopy gave a plate thickness of ~6 nm for W-TBP (Figure 1g) and ~10 nm for Bi-TBP (Figure 1h). To our knowledge, W-TBP is the first W SBU-based MOF.

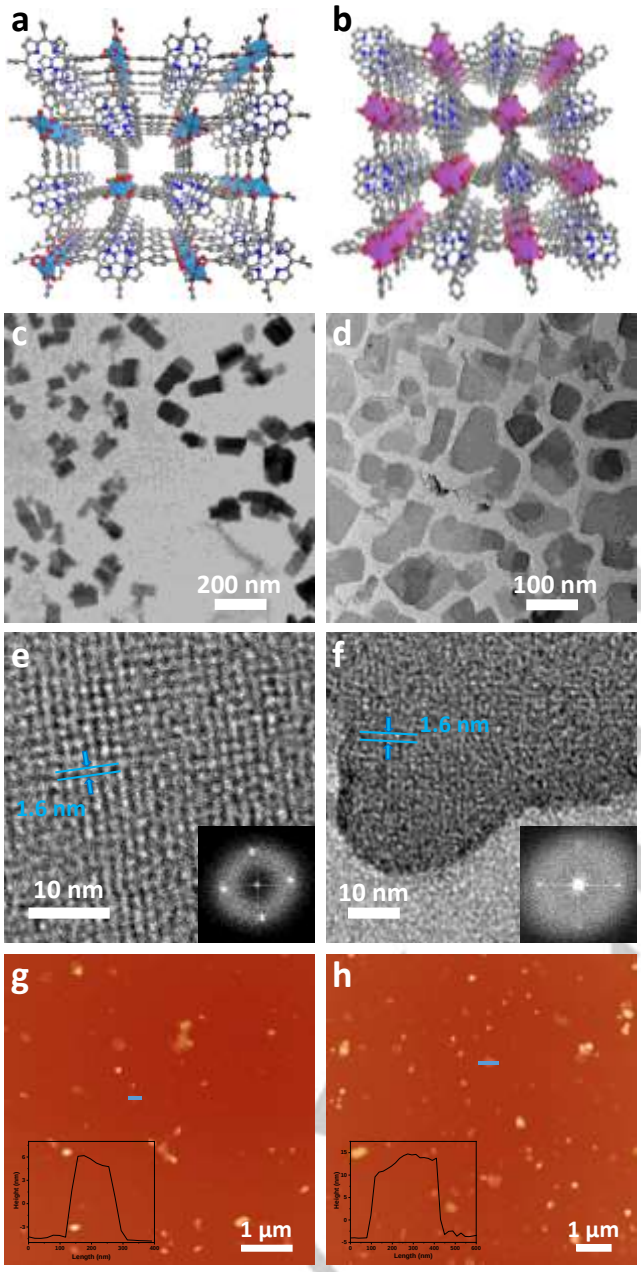

Figure 1. (a,b) Perspective view, (c,d) TEM images, (e,f) HRTEM images and FFT patterns (inset), and (g,h) AFM topography and height profile (inset) of W-TBP (a,c,e) and Bi-TBP (b,d,f) nMOFs, respectively.

PXRD studies revealed that W-TBP is isostructural to previously reported Ru-TBP (Figure 2a and S3),[14] while Bi-TBP has the same structure as its bulk phase whose structure was determined by single crystal X-ray diffraction (Table S1). In W-TBP, TBP ligands are linked by dinuclear W-oxo SBUs to form a cationic 3D framework with a formula of $[W_2(TBP)(H_2O)_2]^{8+}$. In Bi-TBP, TBP ligands are linked by infinite Bi-oxo chains to afford a neutral 3D framework with a formula of $Bi_2(TBP)(O)$ (Figures S1-2). X-ray absorption near edge structure (XANES) of W-TBP indicated the presence of W^{VI} centers (Figure 2b). UV-Vis spectra of W-TBP and Bi-TBP showed four characteristic Q-bands corresponding to non-metalated TBP ligands (Figure 2c). Thermogravimetric analyses (TGA) showed weight losses consistent to the decomposition of W-TBP and Bi-TBP to their respective oxides by 600 °C (Figure S4). Dynamic light scattering (DLS) measurements gave number-average diameters of 114.0 ± 6.7 nm for W-TBP and 125.9 ± 0.7 nm Bi-TBP (Figure 2d).

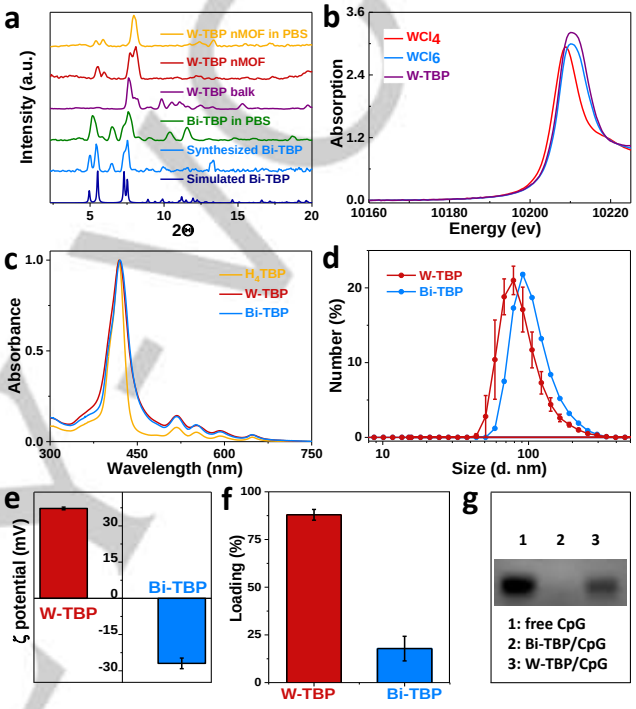

Figure 2. (a) PXRD patterns and stability of W-TBP and Bi-TBP. (b) XANES of W-TBP. (c-e) UV-Vis spectra (c), number-averaged diameters (d), and zeta potential (e) of W-TBP and Bi-TBP. (f, g) CpG loading efficiency (f) and DNA gel of CpG loaded (g) on W-TBP and Bi-TBP.

The cationic framework of W-TBP showed a highly positive zeta-potential of 37.2±0.6 mV (Figure 2e) while the neutral framework of Bi-TBP possessed a negatively charged surface with a zeta-potential of -26.9±2.2 mV. We tested CpG loading by adding 1 μg CpG to a 20 μL PBS solution of W-TBP or Bi-TBP with a TBP concentration of 10 mM. After centrifugation and discarding the supernatants, Bi-TBP adsorbed 17.8% CpG while W-TBP absorbed 87.9% CpG as quantified with a NanoDrop spectrophotometer (Figure 2f). DNA gel electrophoresis of nMOF pellets confirmed more efficient CpG adsorption on W-TBP than Bi-TBP (Figure 2g).

We then tested how nMOFs impact CpG internalization and DC maturation. We first demonstrated efficient TUBO cell uptake of W-TBP and Bi-TBP by time-dependent UV-Vis analysis of TBP absorption (Figure S5). DCs harvested and differentiated from bone marrow cells were then incubated with free CpG, W-TBP, W-TBP/CpG, Bi-TBP, or Bi-TBP/CpG for 72 h. The supernatant was collected and assayed for immunostimulatory cytokines type I Interferon (IFN-α) and interleukin-6 (IL-6) as DC maturation markers. Neither W-TBP nor Bi-TBP alone showed any effect on DC maturation. Only W-TBP/CpG showed elevated IFN-α levels while free CpG and Bi-TBP/CpG had no effect on IFN-α levels (Figure 3a). DCs treated with free CpG excreted IL-6 only in high

10.1002/anie.201911429

WILEY-VCH

COMMUNICATION

CpG concentrations, while DCs treated with W-TBP/CpG excreted IL-6 at low CpG concentrations, indicating enhanced delivery of CpG by cationic W-TBP (Figure 3b).

We next evaluated the cytotoxity of nMOF-mediated PDT on TUBO cells. MTS assay and live/dead cell imaging showed comparable PDT cytotoxicity of W-TBP and Bi-TBP with IC_{50} values of 7.4 ± 0.5 and 5.9 ± 2.2 μM, respectively. In comparison, H_4TBP exhibited an IC_{50} of 16.8 ± 3.4 μM (Figure 3c and S6-8). Confocal imaging and flow cytometric studies further showed that TUBO cells threated with W-TBP or Bi-TBP and light showed high levels of $^1O_2$ generation, cyclooxygenase-2 (COX-2) expression, apoptotic cell death and CRT exposure, indicating PDT-induced immunogenic cell death (ICD) by both nMOFs (Figures S9-16).

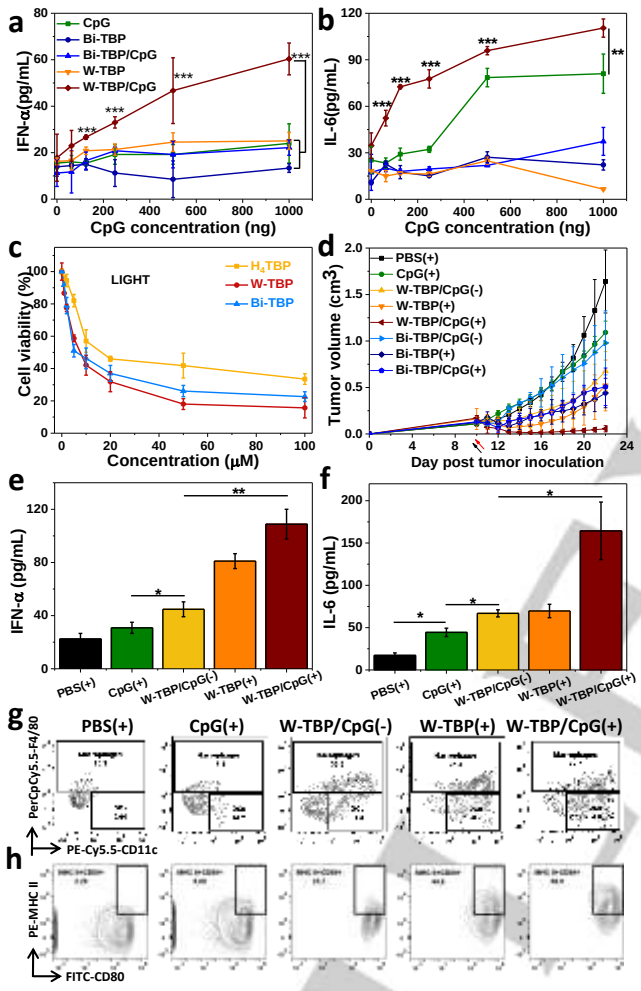

Figure 3. Concentration-dependent IFN-α (a) and IL-6 (b) levels by ELISA. n = 3. (c) Cytotoxicity of H_4TBP, W-TBP or Bi-TBP upon light irradiation. n = 6. (d) In vivo anti-cancer efficacy on single TUBO model. n = 5. ELISA of IFN-α (e) and IL-6 (f) in blood of mice treated as (d). n = 5. Representative figure of tumor-infiltrated macrophage and DC (g) with functional markers MHC-II and CD80 (h). n = 5. Black and red arrows refer to nMOF injection and light irradiation, respectively. *P<0.05, **P<0.01, and ***P<0.001 from control.

The therapeutic effects of local PDT treatment and CpG stimulation mediated by nMOFs were evaluated on a murine breast adenocarcinoma model of TUBO-tumor bearing BALB/c mice. When the tumors reached 150-200 mm^3, PBS, CpG, W-TBP, W-TBP/CpG, Bi-TBP, or Bi-TBP/CpG was injected intratumorally at a TBP dose of 0.2 μmol or/and CpG dose of 1 μg followed by light irradiation (650 nm, 45 J/cm^2). W-TBP/CpG(-) treatment showed enhanced tumor regression over CpG or Bi-TBP/CpG(-) group on Day 22, indicating the ability of cationic W-TBP in stabilizing and delivering CpG to DCs in the TME (Figure 3d). W-TBP(+), Bi-TBP(+) and Bi-TBP/CpG(+) treatments all showed moderate tumor inhibition with no significant difference, suggesting insufficient antitumor efficacy of nMOF-mediated PDT alone. In stark contrast, W-TBP/CpG(+) treatment led to 96.6% tumor regression compared to the PBS group on Day 22, demonstrating a synergistic anti-cancer effect from W-TBP-mediated PDT and CpG delivery. The anti-cancer efficacy was confirmed by optical images and averaged weights of excised tumors on Day 22 (Figure S17-19). Immunofluorescence imaging by terminal deoxynucleotidyl transferase dUTP nick end labeling (TUNEL) and H&E staining indicated severe apoptosis of tumor slices from W-TBP/CpG(+) treatment (Figure S20-21). Steady mouse body weights and the absence of abnormalities on histological images of frozen major organ slices indicated the lack of systemic toxicity for all treatment groups (Figure S22-23).

We also probed innate immune response from various treatments by measuring blood IFN-α and IL-6 concentrations. W-TBP/CpG(-) treatment showed significantly elevated levels of IFN-α and IL-6 over CpG(+) treatment, supporting the role of W-TBP in CpG delivery (Figure 3e&3f). W-TBP/CpG(+) further increased IFN-α and IL-6 levels, consistent with DC maturation by W-TBP-mediated PDT and CpG delivery. Tumor-infiltrating APCs were further analyzed by flow cytometry to confirm the effects of PDT and CpG delivery (Figure S24). W-TBP/CpG(+) significantly increased the populations of macrophages and DCs in the TME over PBS control (Figure 3g and Figures S25-26). DC maturation was further demonstrated with elevated expression of MHC-II and costimulatory CD86 molecules. W-TBP/CpG(+) significantly increased the MHC-II$^+$+CD80$^+$ subset gated on the CD45$^+$CD11b$^+$CD11c$^+$Gr1$^-$F4/80$^-$ population over W-TBP/CpG(-) and PBS(+), indicating enhanced DC functions after W-TBP/CpG(+) treatment (Figures 3h and S27). Finally, W-TBP/CpG(+) showed enlarged tumor-draining lymph nodes (TDLNs), suggesting the presentation of TAAs by DCs and T cell expansion in TDLNs (Figure S28).[8b]

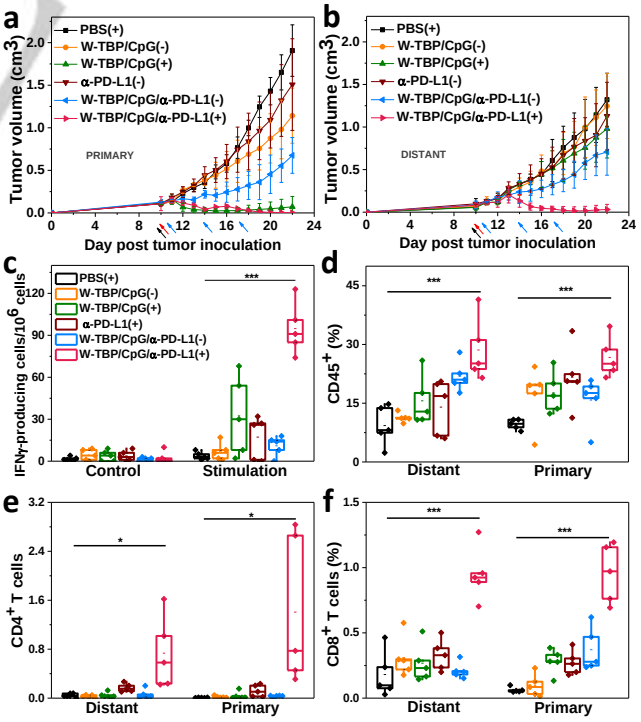

Figure 4. Growth curves of primary tumors (a) and distant tumors (b) of bilateral TUBO tumor-bearing mice. (c) ELISPOT assay showing tumor-specific IFN-γ producing T cells. The percentage of tumor-infiltrating CD45$^+$ cells (d), CD4$^+$ T cells (e), and CD8$^+$ T cells (f) with respect to the total tumor of cells. Black, red

and blue arrows refer to nMOF injection, light irradiation, and α-PD-L1 injection, respectively. The legends in (C) apply to (d-f) as well. N=5. *P<0.05, **P<0.01, and ***P<0.001 from control.

We used a bilateral model of TUBO tumors on BALB/c mice to investigate the synergy between W-TBP/CpG(+)-mediated antigen presentation and systemic CBI. One of the tumors (primary) was treated with W-TBP/CpG with or without light irradiation, while the other tumor (distant) remained untreated. The mice then received intraperitoneal injection of α-PD-L1 antibody (75 μg/mouse). The antitumor efficacy and abscopal effects were assessed by the growth rates of both primary and distant tumors. W-TBP/CpG(+) synergized with α-PD-L1 to elicit consistent abscopal effects, leading to >97% regression of both tumors at a dose of 0.2 μmol based on TBP and light dose of 45 J/cm^2 (Figure 4a&4b). In contrast, W-TBP/CpG/α-PD-L1(-) only elicited slight abscopal effects. As expected, W-TBP/CpG(+) treatment showed strong local tumor control but had almost no effect on distant tumors.

We further examined how W-TBP/CpG(+) enhances CBI. Specific anti-tumor immunity was determined by ELISpot assay. On day 12 post treatment, splenocytes were harvested from TUBO-bearing mice and stimulated with lysed TUBO cells for 42 hours and IFN-γ spot forming cells were counted. The number of antigen-specific IFN-γ producing T cells significantly increased in tumor-bearing mice treated with W-TBP/CpG/α-PD-L1(+) (94.8 ± 18.8 compared to 3.8 ± 2.8 for PBS, Figure 4c). Immune profiling by flow cytometry showed significant increase of tumor-infiltrating leukocytes in both primary and distant tumors in W-TBP/CpG/α-PD-L1(+) group (Figure 4d). W-TBP/CpG/α-PD-L1(+) led to significant neutrophil infiltration on both tumors, suggesting more inflammatory TMEs (Figure S29). W-TBP/CpG/α-PD-L1(+) also significantly increased CD4$^+$ and 8$^+$ T cells in both primary and distant tumors (Figures 4e&4f and S30). W-TBP/CpG(+)-mediated antigen presentation thus synergized with α-PD-L1 to afford strong abscopal effects via immune activation and infiltration of effector T cells.

In summary, we showed that cationic W-TBP combines PDT and CpG delivery to enhance antigen presentation. W-TBP allows for efficient loading of CpG and facile CpG internalization by DCs. W-TBP-mediated PDT induces ICD to release TAAs whereas the delivered CpG enhances DC maturation. The enhanced antigen presentation synergizes with CBI to afford to superb anticancer efficacy and robust abscopal effect with >97% tumor regression in a bilateral breast cancer model. Our work presents a novel strategy to facilitate antigen presentation for cancer immunotherapy using cationic photosensitizing nMOFs.

Acknowledgements

We acknowledge Dr. Zekai Lin for experimental help and the National Cancer Institute (U01-CA198989 and 1R01CA216436) and the University of Chicago Medicine Comprehensive Cancer Center (NIH CCSG: P30 CA014599) for funding support. Single crystal diffraction studies were performed at ChemMatCARS, APS, ANL. NSF's ChemMatCARS Sector 15 is principally supported by the Divisions of Chemistry (CHE) and Materials Research (DMR), National Science Foundation, under grant number NSF/CHE-1346572. Use of the Advanced Photon Source, an Office of Science User Facility operated for the U.S. Department of Energy (DOE) Office of Science by Argonne National Laboratory, was supported by the U.S. DOE under Contract No. DE-AC02-06CH11357.

Keywords: Nanoscale metal-organic framework • Photodynamic therapy • CpG delivery • Antigen presentation • Checkpoint blockade immunotherapy

[1] a) M. J. Smyth, D. I. Godfrey, J. A. Trapani, *Nat. Immunol.* **2001**, *2*, 293-299; b) I. Mellman, G. Coukos, G. Dranoff, *Nature* **2011**, *480*, 480-489.

[2] a) J. R. Brahmer, S. S. Tykodi, L. Q. Chow, W.-J. Hwu, S. L. Topalian, P. Hwu, C. G. Drake, L. H. Camacho, J. Kauh, K. Odunsi, *N. Engl. J. Med.* **2012**, *366*, 2455-2465; b) A. Errico, *Nat. Rev. Clin. Oncol.* **2015**, *12*, 63-63; c) T. Powles, J. P. Eder, G. D. Fine, F. S. Braiteh, Y. Loriot, C. Cruz, J. Bellmunt, H. A. Burris, D. P. Petrylak, S.-l. Teng, *Nature* **2014**, *515*, 558.

[3] a) M. Vanneman, G. Dranoff, *Nat. Rev. Cancer* **2012**, *12*, 237; b) M. J. Smyth, D. I. Godfrey, J. A. Trapani, *Nat. Immunol.* **2001**, *2*, 293.

[4] a) J. Galon, D. Bruni, *Nat. Rev. Drug Discov.* **2019**, 1; b) D. S. Chen, I. Mellman, *Immunity* **2013**, *39*, 1-10.

[5] a) D. E. Dolmans, D. Fukumura, R. K. Jain, *Nat. Rev. Cancer* **2003**, *3*, 380; b) J. F. Lovell, T. W. Liu, J. Chen, G. Zheng, *Chem. Rev.* **2010**, *110*, 2839-2857.

[6] a) L. Galluzzi, A. Buqué, O. Kepp, L. Zitvogel, G. Kroemer, *Nat. Rev.Immunol.* **2017**, *17*, 97; b) A. P. Castano, P. Mroz, M. R. Hamblin, *Nat. Rev. Cancer* **2006**, *6*, 535.

[7] a) J. D. Brody, W. Z. Ai, D. K. Czerwinski, J. A. Torchia, M. Levy, R. H. Advani, Y. H. Kim, R. T. Hoppe, S. J. Knox, L. K. Shin, *J. Clin. Oncol.* **2010**, *28*, 4324; b) N. L. Rosi, D. A. Giljohann, C. S. Thaxton, A. K. Lytton-Jean, M. S. Han, C. A. Mirkin, *Science* **2006**, *312*, 1027-1030; c) G. Hartmann, G. Weiner, A. Krieg, *Proc. Natl. Acad. Sci.* **1999**, *96*, 9305-9310.

[8] a) A. W. Li, M. C. Sobral, S. Badrinath, Y. Choi, A. Graveline, A. G. Stafford, J. C. Weaver, M. O. Dellacherie, T.-Y. Shih, O. A. Ali, *Nat. Mat.* **2018**, *17*, 528; b) H. Liu, K. D. Moynihan, Y. Zheng, G. L. Szeto, A. V. Li, B. Huang, D. S. Van Egeren, C. Park, D. J. Irvine, *Nature* **2014**, *507*, 519; c) G. Zhu, G. M. Lynn, O. Jacobson, K. Chen, Y. Liu, H. Zhang, Y. Ma, F. Zhang, R. Tian, Q. Ni, *Nat.Commun.* **2017**, *8*, 1954.

[9] a) W. Morris, W. E. Briley, E. Auyeung, M. D. Cabezas, C. A. Mirkin, *J. Am. Chem. Soc.* **2014**, *136*, 7261-7264; b) H. Furukawa, K. E. Cordova, M. O'Keeffe, O. M. Yaghi, *Science* **2013**, *341*, 1230444; c) S. L. Anderson, P. G. Boyd, A. Gładysiak, T. N. Nguyen, R. G. Palgrave, D. Kubicki, L. Emsley, D. Bradshaw, M. J. Rosseinsky, B. Smit, *Nat.Commun.* **2019**, *10*, 1612.

[10] a) G. Lan, K. Ni, W. Lin, *Coord. Chem. Rev.* **2019**, *379*, 65-81; b) K. Lu, C. He, W. Lin, *J. Am. Chem. Soc.* **2014**, *136*, 16712-16715; c) G. Lan, K. Ni, Z. Xu, S. S. Veroneau, Y. Song, W. Lin, *J. Am. Chem. Soc.* **2018**, *140*, 5670-5673.

[11] a) K. Lu, C. He, N. Guo, C. Chan, K. Ni, R. R. Weichselbaum, W. Lin, *J. Am. Chem. Soc.* **2016**, *138*, 12502-12510; b) T. C. Johnstone, K. Suntharalingam, S. J. Lippard, *Chem. Rev.* **2016**, *116*, 3436-3486; c) H. Zheng, Y. Zhang, L. Liu, W. Wan, P. Guo, A. M. Nyström, X. Zou, *J. Am. Chem. Soc.* **2016**, *138*, 962-968.

[12] a) F. Lyu, Y. Zhang, R. N. Zare, J. Ge, Z. Liu, *Nano Lett.* **2014**, *14*, 5761-5765; b) F.-K. Shieh, S.-C. Wang, C.-I. Yen, C.-C. Wu, S. Dutta, L.-Y. Chou, J. V. Morabito, P. Hu, M.-H. Hsu, K. C.-W. Wu, *J. Am. Chem. Soc.* **2015**, *137*, 4276-4279.

[13] a) S. Wang, C. M. McGuirk, M. B. Ross, S. Wang, P. Chen, H. Xing, Y. Liu, C. A. Mirkin, *J. Am. Chem. Soc.* **2017**, *139*, 9827-9830; b) Z. Wang, Y. Fu, Z. Kang, X. Liu, N. Chen, Q. Wang, Y. Tu, L. Wang, S. Song, D. Ling, *J. Am. Chem. Soc.* **2017**, *139*, 15784-15791; c) Y. Zhang, C. Liu, F. Wang, Z. Liu, J. Ren, X. Qu, *Chem. Commun.* **2017**, *53*, 1840-1843.

[14] G. Lan, Y.-Y. Zhu, S. S. Veroneau, Z. Xu, D. Micheroni, W. Lin, *J. Am. Chem. Soc.* **2018**, *140*, 5326-5329.

10.1002/anie.201911429

WILEY-VCH

COMMUNICATION

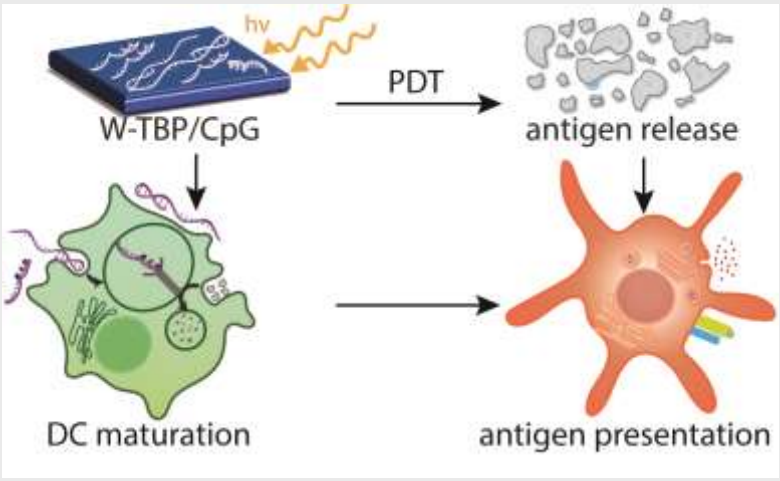

Kaiyuan Ni, Taokun Luo, Guangxu Lan, August Culbert, Yang Song, Tong Wu, Xiaomin Jiang, and Wenbin Lin **

Page 1. – Page 4.

Nanoscale Metal-organic Frameworks Mediate Photodynamic Therapy and Deliver CpG Oligodeoxynucleotides to Enhance Antigen Presentation and Cancer Immunotherapy